RESEARCH ARTICLE

Macromolecular Materials and Engineering Open Access
www.mame-journal.de

A Composite of Polyether Ether Ketone and Silica-Coated Copper Particles for Creating Tailored Conductive Tracks via Laser Printing

Alexander Schnettger, Ulrich Holländer,* and Hans J. Maier**

Conventional substrates for optoelectronic systems include inorganic or organic carrier materials; however, these systems are typically subjected to environmentally harmful multistep processes to prepare printed circuit boards. To mitigate these issues, the present article reports a polyether ether ketone (PEEK)-based composite densely filled with copper microparticles, prepared using a simple, cost-effective, and sustainable synthesis method. The material exhibits high thermal conductivity but is electrically nonconductive prior to undergoing laser treatment. To prevent the composite from exhibiting electrical conductivity, the copper particles are coated with a thin silica layer through a sol–gel reaction. The thermal stability of PEEK and the Cu–PEEK composites with Cu contents of up to 70 vol%, which are prepared via heat melding, is investigated by thermogravimetric analysis, differential scanning calorimetry, and Fourier-transform infrared spectroscopy to clarify the manner in which copper affects the chemical structure of the polymer. The developed composite exhibits a significantly higher thermal conductivity than that of the unfilled PEEK polymer. This paper also describes the effects of laser treatment on the surface morphology. Overall, this study suggests that conductive tracks with low electrical resistance can be created on electrically insulating substrates with high thermal conductivity.

1. Introduction

Metal–thermoplastic composites that can be used as starting materials to create metallic circuit patterns on insulating substrates have recently drawn considerable attention, given their applicability in diverse fields such as light-emitting display production, wearable electronics, bioelectronics, and microelectronics.[1,2] These promising materials combine the beneficial characteristics of metals, such as high thermal and electrical conductivities, with those of thermoplastic polymers, such as design flexibility, chemical stability, light weight, corrosion resistance, and cost- and resource-efficient production.[3] These composites are typically produced by mixing small metal particles with thermoplastic polymer powders, followed by injection molding or extrusion. The thermal and electrical conductivities of these composites are affected by factors such as the concentration, size, shape, and distribution of the metal filler particles. For instance, composites filled with needle-shaped particles can exhibit continuous electrical conductivity even at a low metal content of 10 vol%. This has been attributed to the generation of continuous metal networks due to metal particle agglomeration in the composite. In the case of spherical particles, the metal content is close to the nominal packing density of the spheres.[4]

An insulating layer is typically formed around the metal filler particles to prevent the composites from exhibiting electrical conductivity. Among the typical shell materials used for this purpose—SiO_2, TiO_2, and Al_2O_3[5]—silica is particularly well suited for producing core–shell particles because of its low-cost synthesis; its outstanding properties including optical transparency, chemical inertness, and stability, especially in water; and its amenability to surface modification.[6] For instance, the sol–gel reaction conducted using silicon alkoxides as precursors in ethanol–ammonia mixtures allows the growth of a silica shell around particles.[7,8]

Numerous metallization methods including inkjet printing,[9] photolithography,[10] printed electronics,[11] and ligand-induced electroless plating[12] have been investigated for metallic patterning of thermoplastic surfaces to create conductive tracks. However, these methods typically require toxic solvents, expensive equipment, and complex processing steps.

Laser-induced pattern creation has been targeted as an attractive alternative to the aforementioned methods for fabricating

A. Schnettger, U. Holländer, H. J. Maier
Cluster of Excellence PhoenixD (Photonics, Optics, and Engineering – Innovation Across Disciplines)
Leibniz University Hannover
30167 Hannover, Germany
E-mail: schnettger@iw.uni-hannover.de; hollaender@iw.uni-hannover.de; maier@iw.uni-hannover.de
A. Schnettger, U. Holländer, H. J. Maier
Institute of Materials Science
Leibniz University Hannover
An der Universität 2, 30823 Garbsen, Germany

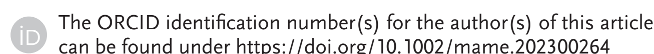
The ORCID identification number(s) for the author(s) of this article can be found under https://doi.org/10.1002/mame.202300264

© 2023 The Authors. Macromolecular Materials and Engineering published by Wiley-VCH GmbH. This is an open access article under the terms of the Creative Commons Attribution License, which permits use, distribution and reproduction in any medium, provided the original work is properly cited.

DOI: 10.1002/mame.202300264

14392054, 2024, 2, Downloaded from https://onlinelibrary.wiley.com/doi/10.1002/mame.202300264 by Cochrane Germany, Wiley Online Library on [08/03/2024]. See the Terms and Conditions (https://onlinelibrary.wiley.com/terms-and-conditions) on Wiley Online Library for rules of use; OA articles are governed by the applicable Creative Commons License

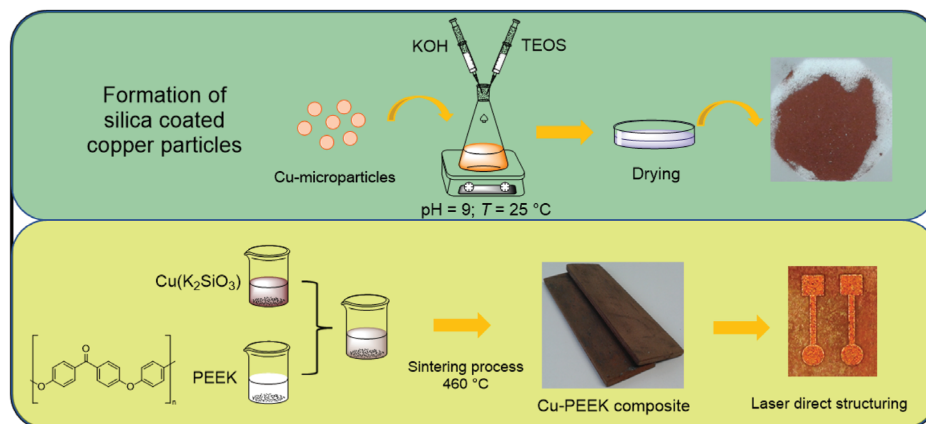

Figure 1. Schematic illustrating the synthesis of silica-coated copper microparticles via a sol–gel reaction and the preparation of the Cu–PEEK composite.

electrically conductive patterns by avoiding multilevel techniques, minimizing costs, and preventing environmental risks.[13] For example, Zhang et al. investigated the formation of copper-based conductive pathways on a composite of copper hydroxyl phosphate [$Cu_2(OH)PO_4$] and acrylonitrile butadiene styrene through laser irradiation, which served as an activation step for the catalytic filler particles, followed by electroless copper plating.[1] Yang et al. prepared a copper aluminate polycarbonate composite and metallized its surface by laser direct structuring, followed by electroless copper plating.[14]

To develop an electrically insulating material with high thermal conductivity as a novel carrier for constructing optoelectronic devices with effective heat dissipation attributes, a metal–thermoplastic composite of polyether ether ketone (PEEK) loaded extensively with spherical copper microparticles was synthesized in the present study.

PEEK, the matrix material of the developed composite, is a polyaromatic, semicrystalline thermoplastic polymer that is synthesized by nucleophilic substitution polycondensation of 4,4′-difluorobenzophenone with the disodium salt of hydroquinone. In particular, PEEK exhibits outstanding mechanical and chemical resistance, even at high temperatures,[15] highlighting its potential for use in heat-dissipating systems. Moreover, it has a glass-transition temperature T_g of 133 °C and a melting temperature T_m of 335 °C, which increase monotonously with increasing ketone-to-ether ratio owing to an improvement in the crystal packing efficiency.[16] Moreover, this aromatic polymer exhibits toughness, abrasion resistance, high impact strength, and particularly noteworthy flexural and tensile properties.[17] In addition, it is resistant to a wide variety of organic solvents.[18]

The desired high content of copper particles in the composite (≈70% by volume) inevitably led to individual particles establishing contact with each other, generating electrically conductive pathways. Thus, to form an insulating silica shell around the particles, a sol–gel reaction was conducted using a high potassium concentration to lower the melting temperature. The silica shell could operate as a fluxing agent, promoting the formation of copper networks via local melting of the surface, which was induced by laser treatment of the surface; this method simultaneously enabled the production of individually designed conductor paths without requiring the subsequent metallization step (**Figure 1**). Specifically, laser direct structuring was employed because it enables noncontact, efficient, and low-cost formation of conductive tracks. In this technique, the laser beam induces selective decomposition of the polymer surface, and the removal of the polymer matrix leads to the formation of a metallic conductive path, with the residual material subjected to only minor thermal and mechanical stresses.[19]

2. Experimental Section

2.1. Chemicals

Tetraethyl orthosilicate (TEOS), ethanol, a concentrated methanolic potassium hydroxide solution, the copper microparticles, PEEK, and potassium hydroxide were obtained from Fisher Scientific GmbH, Scharlau, Acros Organics, GTV GmbH, Goodfellow, and J. T. Baker, respectively. All chemicals were used as received without further purification.

2.2. Synthesis of Silica-Coated Copper Microparticles

Seeded sol–gel polymerization was performed to synthesize nanometer-sized silica coatings for the copper microparticles. To that end, copper particles were first added to an ethanol–water solution with a pH of 9. The pH was adjusted using a concentrated methanolic potassium hydroxide solution. Potassium hydroxide initiated the sol–gel reaction as a catalyst and served as a potassium source to increase the potassium-ion concentration in the shell. Thereafter, a TEOS–ethanol solution was added to the copper–ethanol mixture every 30 min four times. The pH of the resulting solution was maintained by adding potassium hydroxide. The ethanol–water ratio of the solvent was varied from 10:1 to 60:1, the concentration of TEOS was changed from 0.5 to 3 M, and the reaction time was adjusted from 4 to 24 h. The temperature during the reaction was kept constant at 25 °C (Figure 1) Supporting Information).

2.3. Preparation of Cu–PEEK Composite with Silica-Coated Copper Microparticles

Figure 1 demonstrates the procedure for the preparation of the Cu-PEEK composite. The silica-coated copper microparticles and

 © 2023 The Authors. Macromolecular Materials and Engineering published by Wiley-VCH GmbH

Macromolecular Materials and Engineering Open Access
www.mame-journal.de

powdered PEEK (10 μm) were thoroughly mixed in a beaker. The resulting homogeneous mixture was poured into a rectangular steel mold lined with graphite foil, which helped prevent adhesion between the mold and PEEK, and the mold was then covered with another graphite foil. Subsequently, a steel plate was placed on top and the powder was compacted within the mold using a parallel hand press. Finally, the thermoplastic polymer containing the silica-coated copper particles was heat-treated at 470 °C for 1 h in a continuous furnace (Kohnle GmbH, Germany). Subsequently, graphite foil was removed from the obtained silica-coated copper–PEEK composite.

2.4. Differential Scanning Calorimetry (DSC)

DSC measurements of the composite (≈5 mg) were performed using a NETZSCH DSC 214 device (Polyma, Germany) in a nitrogen atmosphere by increasing the temperature from 30 to 400 °C at a heating rate of 10 °C min^{-1} in an aluminum oxide pan. The DSC curves of PEEK and the PEEK/silica-coated copper composites with different copper concentrations (65 and 70 vol%) helped determine the glass transition temperature and melting range of the polymer.

2.5. Thermogravimetric Analysis (TGA)

The copper–PEEK composite (≈15 g) was subjected to TGA using a NETZSCH TG 209 F1 Libra apparatus by increasing the temperature from 30 to 900 °C in a nitrogen atmosphere and from 900 to 1000 °C in an oxygen atmosphere at a heating rate of 10 °C min^{-1} in an aluminum oxide pan.

2.6. Fourier-Transform Infrared (FTIR) Spectroscopy

FTIR spectra of the silica-coated microparticles and copper–PEEK composites were acquired using a LUMOS II system (Bruker, Germany). Owing to the opacity of the samples, the copper–PEEK composites were crushed and filled with potassium bromide pellets. Spectra of the composites were collected in attenuated-total-reflection mode and those of the particles were acquired in transmission mode at a resolution of 2 cm^{-1} with 30 scans per measurement in the range of 400–4000 cm^{-1}.

2.7. Scanning Electron Microscopy (SEM)

The silica-coated copper microparticles were characterized by SEM to examine the structure and thickness of the silica shell, with the latter determined by inspecting the silica layer from the coating edges to uncoated areas. The layer thickness was estimated by correlating the experimentally measured value with the Si/Cu ratio of the coated particles. SEM was performed using a ZEISS Supra 55 VP instrument operating at 15 kV by applying powdered samples onto carbon platelets. Energy-dispersive X-ray (EDX) spectroscopy was performed to determine the chemical composition of the silica shells, with elemental mapping analysis conducted to probe the elemental distributions on the copper surface.

2.8. Laser Treatment

The laser treatment of the Cu–PEEK composite surface, which helped generate conductive tracks, was performed using a DPL Smart Marker II system featuring a Nd:YAG laser (ACI Laser GmbH) in air with a wavelength of 1064 nm, a maximum power of 10 W, a repetition rate of 80 kHz, and a spot size of 50 μm. The parameters power (1.6–8.4 W corresponds to 40%–100%), frequency (30–80 kHz), writing speed (600–1100 mm s^{-1}), and number of repetitions (1–5) were set using Magic Mark (V.3) software.

2.9. Thermal Conductivity

The thermal diffusivity (α) values of the composite and pure PEEK (α) were determined from thermal conductivity measurements as follows

$$\alpha = \frac{\lambda}{\rho \cdot c} \tag{1}$$

where λ is the thermal conductivity, ρ is the density, and c is the specific heat capacity. The thermal conductivity measurements were performed using a NETZSCH LFA 447 instrument, in which the bottom of the sample was subjected to a short heating pulse using a xenon flash lamp. An infrared detector was placed on the upper side to measure heat increase. Thermal conductivity was measured at temperatures of 25, 50, 100, 150, and 200 °C.

3. Results and Discussion

3.1. Synthesis of Silica-Coated Copper Microparticles

SEM imaging of the silica-coated copper microparticles (**Figure 2**a) revealed that most of the copper particles were covered with a dense silica shell. The dark gray and lighter areas on the particle surface corresponded to silica and uncoated copper, respectively. Elemental mapping analysis suggested that a dense layer comprising silicon, oxygen, and potassium had formed on most of the copper particle surfaces (Figure 2c–f). The formation of a silica layer on the copper surface is determined by the interaction between copper atoms and the silica molecules. A crystalline copper surface is not able to form strong adhesion with the silica; in this case, the interaction is based on electrostatic effects. The partial oxidation of the copper surface results in a chemical bond between the oxygen atom of the copper oxide and the silicon atom. In the Cu-PEEK composite material, adhesion is determined by the intermolecular interaction between PEEK and the silica. The presence of hydroxyl groups on the surface of the silica layer leads to the formation of hydrogen bonds with the carbonyl group of the PEEK polymer molecule.

SEM was also used to determine the thickness of the silica shell. The silica shell thickness was measured at different parts of a particle and on different particles at the edge of coated and uncoated areas. The received average shell thicknesses were correlated with the silicon copper ratio determined by EDX analysis of the examined samples. The mean silica layer thickness of the

© 2023 The Authors. Macromolecular Materials and Engineering published by Wiley-VCH GmbH

14392054, 2024, 2, Downloaded from https://onlinelibrary.wiley.com/doi/10.1002/mame.202300264 by Cochrane Germany, Wiley Online Library on [08/03/2024]. See the Terms and Conditions (https://onlinelibrary.wiley.com/terms-and-conditions) on Wiley Online Library for rules of use; OA articles are governed by the applicable Creative Commons License

14392054, 2024, 2, Downloaded from https://onlinelibrary.wiley.com/doi/10.1002/mame.202300264 by Cochrane Germany, Wiley Online Library on [08/03/2024]. See the Terms and Conditions (https://onlinelibrary.wiley.com/terms-and-conditions) on Wiley Online Library for rules of use; OA articles are governed by the applicable Creative Commons License

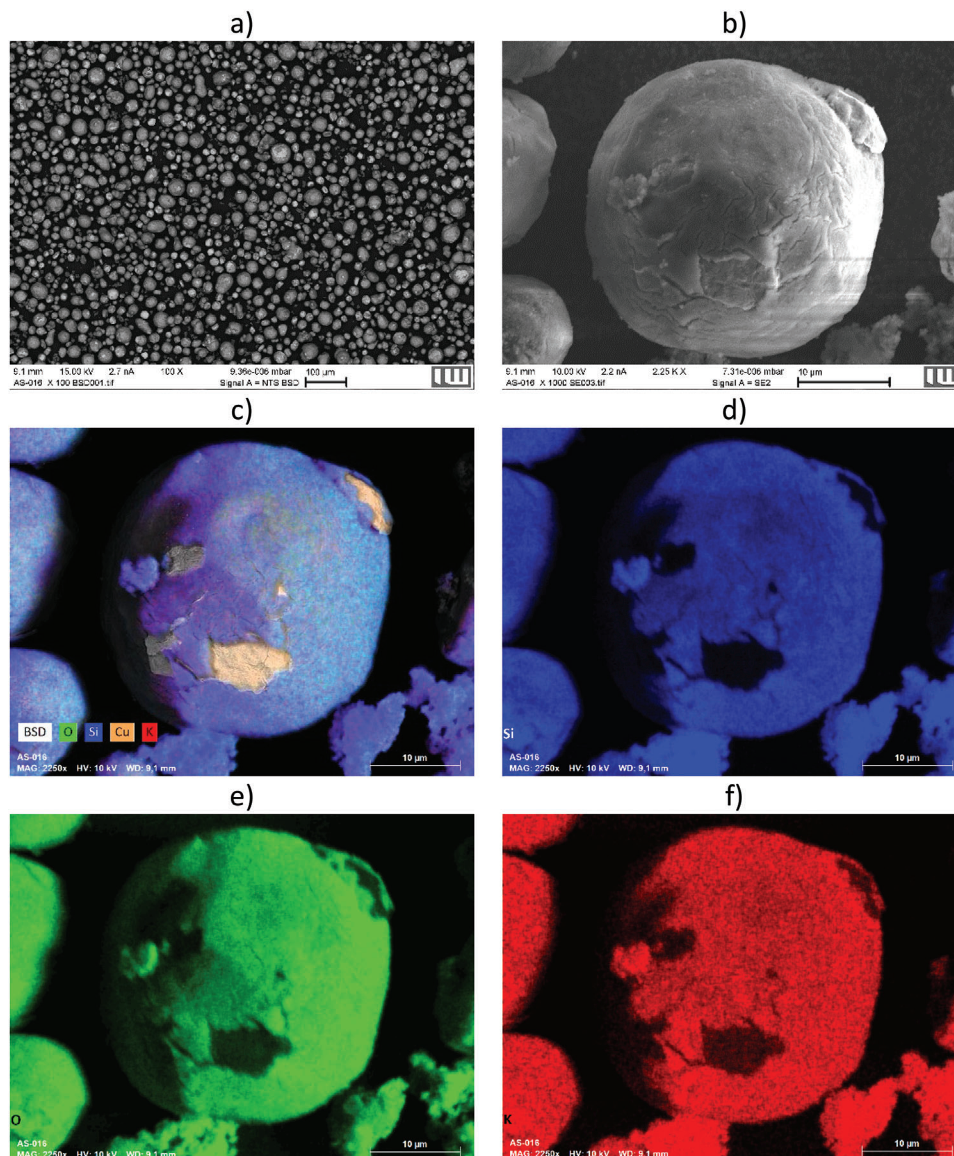

Figure 2. SEM images and elemental maps of the silica-coated copper microparticles: a) wide-area image demonstrating the difference in particle size; b) high-magnification image of a single K_2SiO_3-coated copper particle; and distributions of c) all four elements (O, Si, Cu, and K), d) Si, e) O, and f) K on the surface of a representative copper particle.

particles was calculated using Equation (2)

$$x = \frac{r_{\mathrm{Si:Cu},2}}{r_{\mathrm{Si:Cu},1}} \cdot x_1 \tag{2}$$

where x_1 is the measured silica shell thickness, $r_{\mathrm{Si:Cu},1}$ is the molar ratio of the area where the layer thickness was determined, and $r_{\mathrm{Si:Cu},2}$ is the molar ratio of the silica coated particles. The calculated silica shell thicknesses are summarized in **Table 1**.

Essentially, a representative silica-coated copper microparticle with uncoated areas was used to measure the layer thickness (**Figure 3**), which was estimated to be 300–560 nm.

FTIR analysis of the silica-coated copper particles was performed to validate the surface functionalization of the copper particles (**Figure 4**). In the acquired spectrum, the IR band at 782 cm^{-1} is associated with Si—OH and Si—O bonds. Moreover, the intense peak at 1045 cm^{-1} signifies the asymmetrical stretching vibration of Si—O—Si bonds, and the peak at 3450 cm^{-1} corresponds to the O—H stretching vibration.[20,8]

The present study was primarily aimed at optimizing the reaction conditions for achieving a homogenous silica coating with a high potassium concentration. The melting point of silica depends on the potassium concentration in the polymeric network,[21] with an increase in potassium concentration leading to a decrease in the melting temperature. Ammonia, which is typically used as a catalyst in sol–gel reactions, was not employed in the present study owing to its tendency to form copper tetraamine complexes $[Cu(NH_3)_4]^{2+}$.[22] Therefore, potassium hydroxide was used instead of ammonia as the catalyst and also as the potassium source. The hydrolysis and condensation steps

 © 2023 The Authors. Macromolecular Materials and Engineering published by Wiley-VCH GmbH

Table 1. Reaction conditions for coating copper microparticles with silica and the corresponding silica shell thicknesses and silica-to-potassium ratios

No.	Preparation conditions			Results	
	t [h]	*c* [mol L^{-1}]	EtOH/H$_2$0	Shell thickness [nm]	Si/K ratio[a)]
1	4	0.5	60	70	2.8
2	4	0.5	35	90	2.1
3	4	0.5	10	130	2.5
4	4	1.75	60	70	2.9
5	4	1.75	35	280	4.4
6	4	1.75	10	210	2.9
7	4	3	60	710	4.2
8	4	3	35	140	2.9
9	4	3	10	50	2.8
10	24	0.5	60	290	2.8
11	24	0.5	35	250	3.3
12	24	0.5	10	5	2.5
13	24	1.75	60	5	1.8
14	24	1.75	35	6	3.1
15	24	1.75	10	7	3.4
16	24	3	35	200	3.3
17	24	3	10	6	2.8
18	9	0.5	60	30	3.1
19	9	0.5	35	80	3.1
20	9	0.5	10	90	3.1
21	9	1.75	60	40	3.0
22	9	1.75	35	50	3.7
23	9	1.75	10	90	3.1
24	9	3	60	80	3.6
25	9	3	35	160	2.8
26	9	3	10	40	2.9

[a)] Si/K ratio determined based on the mass percent estimated from EDX analysis.

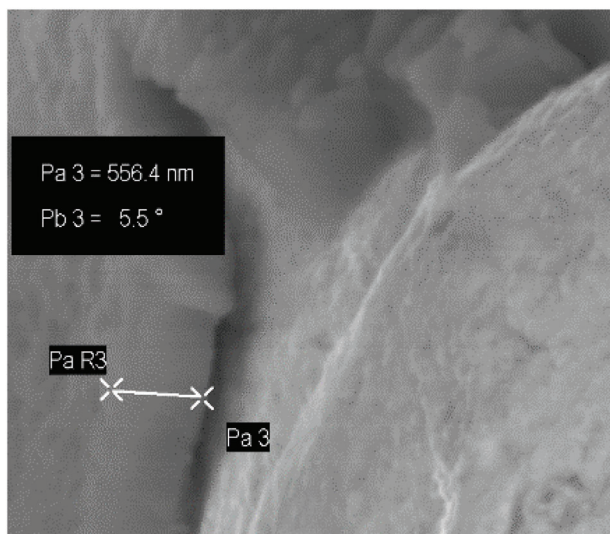

Figure 3. Silica shell thickness determined by inspecting the silica layer at the edge between coated and uncoated areas.

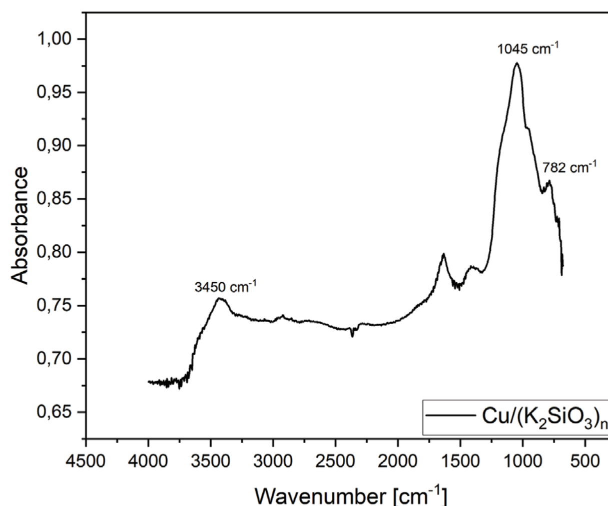

Figure 4. FTIR spectrum of silica-coated copper microparticles in KBr pellets.

of sol–gel reactions are strongly affected by the process parameters, with branched cluster formation, hydrolysis, and condensation occurring faster under basic conditions than under acidic conditions.[23] Therefore, the reaction time, concentration of the silica precursor (TEOS), and ethanol-to-water ratio were varied to optimize the reaction conditions. The temperature and pH of the solution (9) were kept constant. According to Liz-Marzán et al., the pH should be maintained between 8 and 10 to reduce the solubility of the silicate species in the solution and avoid the formation of silica nuclei instead of a dense silica layer.[24] The reaction conditions and the calculated thickness of the silica shell for different silica-to-potassium ratios, which describe the amount of potassium in the shell, are summarized in Table 1.

When the reaction was conducted for 4 h, the shell became thicker as the TEOS concentration increased, from 70 nm at 0.5 M TEOS to 710 nm at 3 M TEOS. Moreover, for a fixed reaction time and TEOS concentration, the thickness of the silica layer increased with increasing water content. According to Kobayashi et al.[7] and Mine et al.,[25] an increase in water concentration increases the shell thickness, owing to the dissociation of ammonia hydroxide, and increases the ionic strength of the solution. The layer thickness obtained using a TEOS concentration of 0.5 M in the 4 h reaction increased from 70 to 130 nm when the ethanol-to-water ratio was changed from 60:1 to 10:1. Evidently, the higher water concentration increased the hydrolysis rate of the ethoxy groups of the TEOS molecules, yielding silanol groups. The hydrolysis step of the sol–gel reaction occurs via an S_N2-Si mechanism involving the attack of a hydroxide ion on the silicon atom and replacement of the alkoxide anion by inversion of the silicon tetrahedron.[26] At a high H_2O concentration, the silicon precursor is completely hydrolyzed, and more silanol groups are available for the condensation step and agglomerate into larger shells on the surface of the copper particles.[27,28] Notably, the silica-to-potassium ratio increased with increasing shell thickness, and a decrease in the potassium concentration in the shell led to an increase in the melting temperature of the silica layer.

Furthermore, the silica shell obtained via prolonged reactions was found to be thinner, in contrast to our expectations and

 © 2023 The Authors. Macromolecular Materials and Engineering published by Wiley-VCH GmbH

14392054, 2024, 2, Downloaded from https://onlinelibrary.wiley.com/doi/10.1002/mame.202300264 by Cochrane Germany, Wiley Online Library on [08/03/2024]. See the Terms and Conditions (https://onlinelibrary.wiley.com/terms-and-conditions) on Wiley Online Library for rules of use; OA articles are governed by the applicable Creative Commons License

Macromolecular Materials and Engineering Open Access
www.mame-journal.de

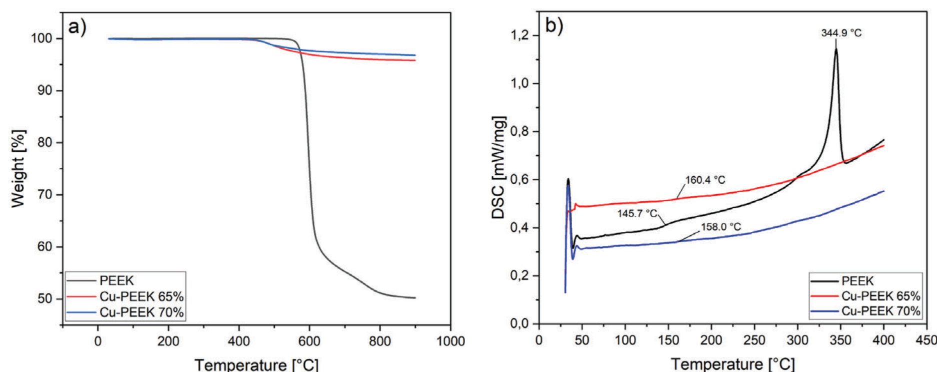

Figure 5. a) TGA and b) DSC curves of PEEK and Cu–PEEK composites containing 65 and 70 vol% silica-coated copper microparticles, obtained in a nitrogen atmosphere.

previously reported results.[29] This was presumably due to the friction between the copper particles, which shaved off the silica layer from the surface. Furthermore, core-free silica spheres arise from secondary nucleation during the sol–gel reaction consuming TEOS, which cannot be deposited onto the copper particles.[28] Overall, the optimal conditions for performing the sol–gel reaction to yield a dense, thin layer with a high potassium concentration were as follows: reaction time, 4 h; TEOS concentration, 0.5 M; and ethanol-to-water ratio, 35:1. The corresponding reaction yielded a 90-nm-thick shell and a silicon-to-potassium ratio of 2.04, resulting in a melting temperature of ≈800 °C.

3.2. TGA of the Cu–PEEK Composite

The thermal stability of PEEK and the copper–PEEK composites containing silica-coated copper microparticles of different concentrations was assessed by TGA in an inert atmosphere (**Figure 5**a). The TGA curve of pristine PEEK showed that the polymer was not affected by the increase in temperature up to the initial stage of decomposition, which occurred at 520 °C. Notably, decomposition of the Cu–PEEK composite with 65 vol% copper was initiated at 410 °C. A further increase in the Cu content of the polymer matrix to 70 vol% reduced the temperature at which decomposition was initiated to 400 °C.

Pristine PEEK decomposed rapidly and significantly from 550 to 618 °C, leading to a weight loss of 38%. The decomposition rate decreased at temperatures above 620 °C, leading to a maximal weight loss of 50% at 900 °C. Vasconcelos et al. observed similar thermal behavior when investigating neat PEEK in a nitrogen atmosphere.[30] Notably, in contrast to the considerable maximum weight loss of pristine PEEK, that of the Cu–PEEK composite containing 70 vol% copper was only 3.3% at 900 °C, with the composite containing 65 vol% copper exhibiting a slightly higher value of 4.2%. The weight loss of the composites was significantly lower than that of the PEEK polymer matrix (≈50%). The thermal decomposition of PEEK occurs in two steps, with the first step involving chain scission of the ether and ketone bonds, yielding phenol as the main decomposition product, and the slower second step involving volatilization of the decomposition product residue and carbonization of the leftover residue. Patel et al. comprehensively described the decomposition of PEEK through a radical decomposition reaction.[31] The incorporation of copper into thermoplastic PEEK led to reduced thermal stability owing to the weakening of chain interactions and the loss of polymer chain flexibility.[32] However, the presence of a high copper content essentially led to a lower weight loss because copper did not melt in the investigated temperature range. Another factor that caused the low weight loss was the barrier effect of the incorporated copper microparticles, which hindered the diffusion of the polymer decomposition products from the condensed phase to the gas phase.

3.3. DSC Analysis

The thermal behavior of thermoplastic PEEK and the Cu–PEEK composites containing 65 and 70 vol% silica-coated copper microparticles was further examined by acquiring thermograms (Figure 5b). The T_g values of the Cu–PEEK composites (160.4 °C for Cu–PEEK 65 vol% and 158 °C for Cu–PEEK 70 vol%) were higher than that of pristine PEEK (145.7°C). The copper microparticles in the composite limited the mobility of the polymer chains by reducing the free volume of the PEEK matrix. According to Droste and Dibenedetto, the flexibility and mobility of the polymer chain are reduced by the filler–polymer matrix interactions, and the T_g enhancement depends on the type and concentration of the filler.[33] Atkinson et al. analyzed the increase in T_g based on crystallinity, which limits the polymer chain mobility, and noted that highly crystalline areas of a polymer exhibit a higher T_g than that of semicrystalline regions.[34] PEEK exhibits a T_m value of 344.9 °C and a melting enthalpy ΔH_m of 44 J g^{-1}. Notably, in contrast to PEEK, the Cu–PEEK composites did not exhibit melting behavior. Copper did not melt in the investigated temperature range, and the first-order thermal transformation of PEEK melting was not detected owing to the high copper content in the composite (65–70 vol%). In addition, certain parts of PEEK could have existed in an amorphous state. Al-Khazaal and Ahmad argued that increasing the metal content increases the heat of fusion, leading to the composite exhibiting superior adhesive properties.[35]

3.4. FTIR Spectroscopy

FTIR spectra of PEEK and the Cu–PEEK composites with copper contents of 65 and 70 vol% were acquired (**Figure 6**). The spectra

 © 2023 The Authors. Macromolecular Materials and Engineering published by Wiley-VCH GmbH

14392054, 2024, 2, Downloaded from https://onlinelibrary.wiley.com/doi/10.1002/mame.202300264 by Cochrane Germany, Wiley Online Library on [08/03/2024]. See the Terms and Conditions (https://onlinelibrary.wiley.com/terms-and-conditions) on Wiley Online Library for rules of use; OA articles are governed by the applicable Creative Commons License

Macromolecular Materials and Engineering Open Access
www.mame-journal.de

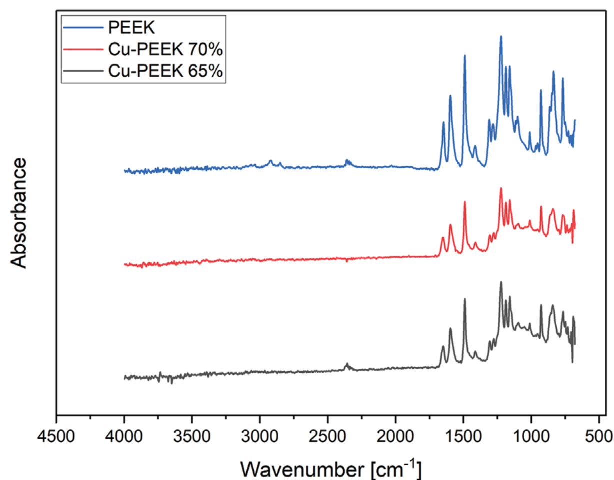

Figure 6. FTIR spectra of PEEK and the Cu–PEEK composites containing 65 and 70 vol% silica-coated copper microparticles.

showed different peak intensities that decreased with increasing copper content. Copper neither affected the chemical structure of the polymer nor catalyzed its decomposition during the composite preparation. In the obtained spectra, the absorption peak at 2933 cm^{-1} represents the stretching vibration of C—H bonds in the aromatic rings. Moreover, the peak at 1645 cm^{-1} is indicative of the C=O stretching vibration of the carbonyl unit, and the band at 1223 cm^{-1} can be attributed to the C—O—C asymmetric stretching vibrations of the ether bond between the two phenyl groups. The adsorption peaks appearing at wavenumbers below 1000 cm^{-1} represent the distinctive fingerprint peaks of PEEK, which are consistent with the literature.[36]

3.5. Formation of Conductive Tracks via Laser Treatment

Laser treatment of the surface of an insulating thermoplastic composite can enable selective metallization to achieve a smooth metal surface by fusing neat copper particles. The direct metallization of the surface by means of laser marking allows great freedom in the design of the marking pattern. Due to the favored application of the composite material as a basis for conductor paths, the lasered structures are preferably lines, squares and circles, which serve as possible connection points (**Figure 7**). This approach permits the creation of conductive tracks on a composite surface in a single step. The successful preparation of conductive tracks by laser melting depends on the content and shape of the metal particles and their dispersion within the polymer matrix. Notably, short circuits can occur between the conductive tracks in systems with a high metal content.[37] Thus, an insulating silica shell is necessary around the copper particles, which helps the surrounding material retain its nonconductive properties.

In the present study, the formation of a smooth, closed metal surface with low electrical resistance was assessed by pyrolyzing the polymer and silicate layer and fusing the copper particles by tuning the laser treatment parameters. In particular, the power, frequency, writing speed, and number of repetitions were varied to determine the optimal conditions. The laser irradiation effects are related to the amount of energy provided to the surface of the composite and the selected processing parameters.

Within the scope of the study conductive tracks with a width of 1.2 ± 0.01 mm and a length of 10 ± 0.01 mm can be produced. Due to the high electrical resistance of the composite material of 1.5 MΩ, which is achieved by the silica layer on the surface of the copper particles, the distance between the lasered tracks could be reduced to 0.4 mm without causing short circuits between the individual tracks. The dependence of the electrical resistance of the generated conductive path on frequency was investigated for different laser powers ranging from 40% to 60% at a constant writing speed of 150 mm s^{-1} (**Figure 8**a). The results did not reveal a clear trend with respect to the increase in pulse repetition frequency. When the surface of the composite was structured using a laser power of 60%, the electrical resistance initially decreased significantly to 0.28 kΩ. This value is distinctly higher than that of neat copper and the targeted electrical resistance of <1 Ω due to absent particle agglomeration and fusion. The electrical resistance of the generated conductive path increased with further increases in frequency, reaching a maximum at 55 000 Hz. The fluctuating trends were presumably related to the distribution of copper particles in the polymer. The particles were heated to different degrees owing to the different sizes of the copper particles and variations in their distribution; this temperature gradient had a limiting influence on the melting behavior.[38]

The electrical resistance was then examined as a function of the laser power at a constant frequency of 60 000 Hz and a writing speed of 300 mm s^{-1} (Figure 8b). Increasing the laser power from 40% to 50% led to a decrease in the electrical resistance to 0.46 kΩ, with subsequent increases in the laser power leading to an increase in the electrical resistance to 1.1 kΩ. The high energy input not only led to the decomposition of the silica shell, but also resulted in the silica coating fusing with the glassy structures between the copper particles, thereby decreasing the electrical conductivity (**Figure 9**f). Hou et al. observed the opposite behavior,

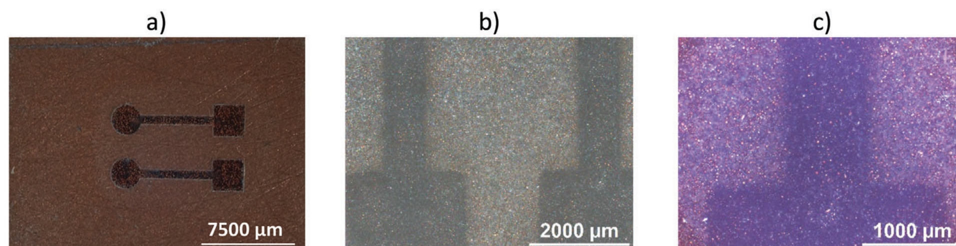

Figure 7. a) Lasered conductive track on Cu-PEEK composite containing 70% silica-coated copper particles; b,c) optical microscope images of the lasered conductive tracks.

© 2023 The Authors. Macromolecular Materials and Engineering published by Wiley-VCH GmbH

14392054, 2024, 2, Downloaded from https://onlinelibrary.wiley.com/doi/10.1002/mame.202300264 by Cochrane Germany, Wiley Online Library on [08/03/2024]. See the Terms and Conditions (https://onlinelibrary.wiley.com/terms-and-conditions) on Wiley Online Library for rules of use; OA articles are governed by the applicable Creative Commons License

14392054, 2024, 2, Downloaded from https://onlinelibrary.wiley.com/doi/10.1002/mame.202300264 by Cochrane Germany, Wiley Online Library on [08/03/2024]. See the Terms and Conditions (https://onlinelibrary.wiley.com/terms-and-conditions) on Wiley Online Library for rules of use; OA articles are governed by the applicable Creative Commons License

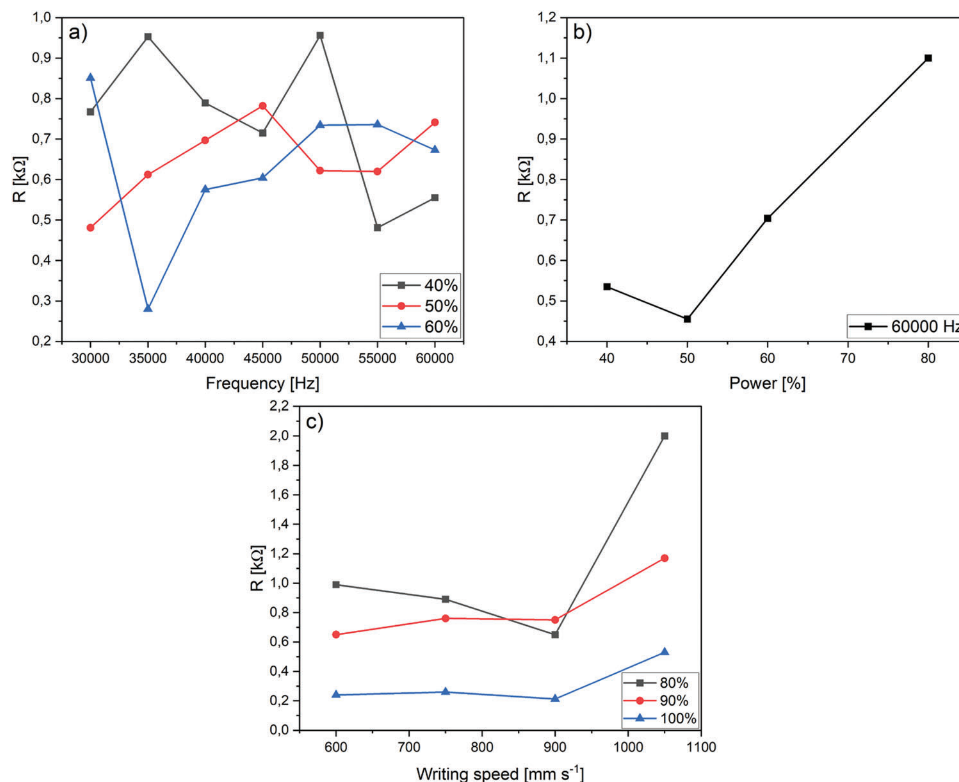

Figure 8. Electrical resistance of the laser-treatment-derived conductive tracks for a) different pulse repetition frequencies and three different laser powers, b) different laser powers at a high frequency of 60 kHz, and c) different writing speeds for laser powers between 80% and 100%.

in that an increase in the laser power decreased the electrical resistance of the laser-generated conductive track. Their composite comprised high-density polyethylene and copper particles without insulating layers.[39]

The electrical resistance of the traces was then probed as a function of the writing speed at a fixed frequency (Figure 8c). Increasing the laser power from 80% to 100% led to a decrease in the electrical resistance. Moreover, the writing speed of the laser in the range of 600–900 mm s^{-1} did not affect the electrical resistance; however, a further increase in the writing speed to 1050 mm s^{-1} enhanced the electrical resistance. These trends have been reported in studies on the formation of conductive structures on composite surfaces.[39,40] The aforementioned result indicates that individual areas could no longer be sufficiently heated by increasing the writing speed, implying that the copper particles did not fuse together.[41]

Overall, these results show that the formation of conductive tracks on a copper–PEEK composite surface could be achieved by single-step metallization through laser direct writing, in contrast to the more complicated procedure reported by Xu et al., which involved laser activation of the surface, followed by cleaning with different solvents and electroless plating.[13] The dimensions of the obtained lasered structures do not meet the level of manufactured conductive tracks, which attain linewidth of 50 µm. Further work is needed to reduce the linewidth and to improve the electrical conductivity. Different insulating polymer coatings such as polydimethylsiloxane (PDMS) with a lower decomposition temperature compared to silica and which pyrolyze during laser treatment need to be investigated to reduce residues among the copper particles. The apparent properties of PDMS polymer are chemical stability, electrical insulation, functional processing, high transparency, and flexibility.[13] However, this method offers the opportunity to create manifold metallized structures on a surface.

3.6. Morphologies of the Untreated and Laser-Irradiated Composites

To probe the effects of laser irradiation on the morphology of the Cu–PEEK composites, SEM images of the surface were acquired before and after laser treatment with an Nd:YAG laser. The surface of the Cu–PEEK composite with 70 vol% copper particles before and after laser irradiation was imaged, and Cu and Si maps were acquired (Figure 9). As shown in the wide-area micrographs, the copper microparticles were uniformly distributed in the composite and partially covered and separated by a PEEK layer. In the SEM images of the laser-irradiated composite (Figure 9c,d), the low-magnification image provided evidence of the decomposition of the polymer matrix. Laser irradiation led to the degradation of PEEK via pyrolysis, and only the copper particles remained. The copper particles fused owing to the thermal effect, which increased the particle diameter; in a few cases, the particles even fused into elongated units. This clearly indicated that the selected laser parameters were insufficient for overcoming the surface tension of the copper particles to form a

 © 2023 The Authors. Macromolecular Materials and Engineering published by Wiley-VCH GmbH

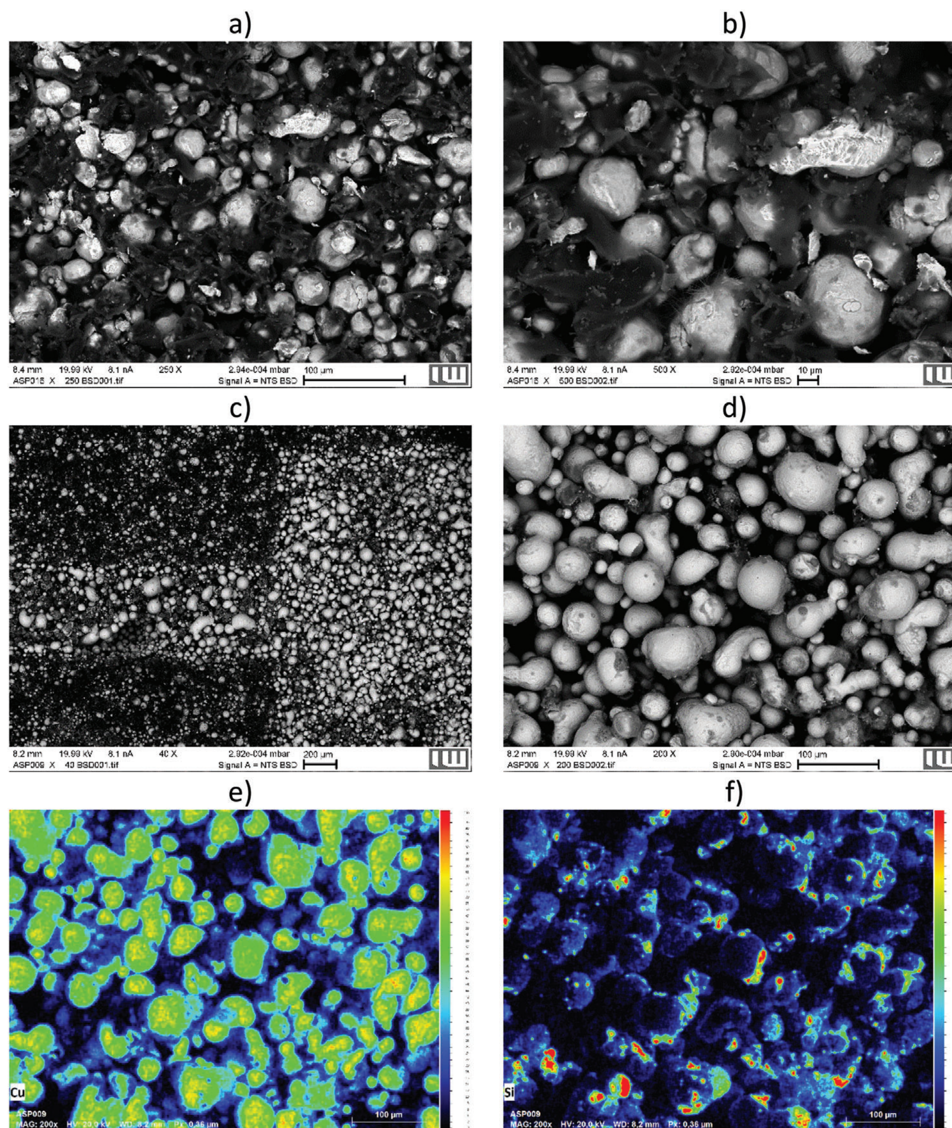

Figure 9. SEM images of the Cu–PEEK composite (70%): a,c) wide-area and b,d) high-magnification images of the a,b) untreated and c,d) laser-treated specimens, and elemental maps of e) Cu and f) Si in the laser-treated sample.

conductive track. Caradonna et al. observed a strong dependence between the laser setup, track morphology, and the electrical behavior of the track.[42] Analysis of the silicon distribution on the surface of the copper particles after laser treatment (Figure 9f) indicated the occurrence of silica shell pyrolysis on the surface and the lack of a fluxing effect for merging the copper particles. The residual silica on the sides of the particles resulted in locally insulating properties, that is, a decrease in macroscopic electric conductivity.

3.7. Thermal Conductivities of PEEK and the Cu–PEEK Composite

Polymers typically exhibit low thermal conductivity, thereby necessitating the development of polymer composites with thermally conductive fillers, such as copper microparticles, to realize thermally conductive polymer systems. Therefore, in this study, the influences of filler concentration and particle size on the thermal conductivity of PEEK were investigated.

The thermal conductivity of the unfilled PEEK polymer at 25 °C, 0.275 W m^{-1} K^{-1}, decreased minimally to 0.2 W m^{-1} K^{-1} at 200 °C (**Figure 10**). The thermal conductivity of PEEK remained almost constant in the considered temperature range because the intermolecular interactions of this thermally stable semicrystalline isotropic polymer were not substantially affected by the temperature increase. The primary heat transfer mechanism in PEEK involves phonon transport and phonon scattering inside the polymer matrix, with the morphology affecting the heat conduction. The addition of 65 vol% 45-µm-sized copper microparticles to PEEK led to an ≈650% increase in thermal conductivity to 2.07 W m^{-1} K^{-1} compared with that of the pristine sample. Rivière et al. also observed an increase in the thermal

 © 2023 The Authors. Macromolecular Materials and Engineering published by Wiley-VCH GmbH

14392054, 2024, 2, Downloaded from https://onlinelibrary.wiley.com/doi/10.1002/mame.202300264 by Cochrane Germany, Wiley Online Library on [08/03/2024]. See the Terms and Conditions (https://onlinelibrary.wiley.com/terms-and-conditions) on Wiley Online Library for rules of use; OA articles are governed by the applicable Creative Commons License

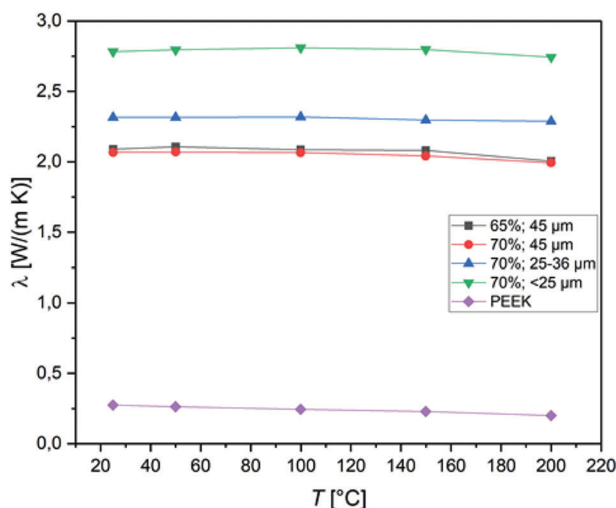

Figure 10. Temperature-dependent thermal conductivity of PEEK and the Cu–PEEK composites with filler concentrations of 65 and 70 vol% for different particle sizes between <25 and 45 µm.

conductivity of PEEK composites with increasing silver filler content.[43] In the present study, the copper microparticles established contact owing to their high concentration in the polymer, thereby creating a thermally conductive pathway. These contacts between the copper particles necessitated the addition of an insulating silica coating to prevent them from exhibiting electrical conductivity prior to laser treatment.

A further increase in the content of 45-µm-sized copper microparticles to 70 vol% led a slight increase in thermal conductivity. However, the thermal conductivity remained relatively constant in the considered temperature range, presumably owing to phonon scattering in crystalline materials and a lack of the filler–polymer matrix interactions.[44] The filler size significantly affected the thermal conductivity of the composites, with a reduction in the copper microparticle size leading to an increase in heat conduction. The Cu–PEEK composite with 70 vol% 25–36-µm-sized copper particles exhibited a thermal conductivity of 2.32 W m^{-1} K^{-1}. Smaller particles can be packed more tightly, thereby yielding efficient thermally conductive pathways in metal–thermoplastic composites.[45] A further decrease in the particle size to less than 25 µm and a filler loading of 70 vol% led a considerably higher thermal conductivity of 2.78 W m^{-1} K^{-1}. These results clearly demonstrate that increasing the filler content and decreasing the particle size led to the formation of a well-connected filler network throughout the PEEK matrix, which consequently increased the thermal conductivity.

4. Conclusion

A PEEK-based composite filled extensively with copper microparticles, which exhibited high thermal conductivity and electrical insulating behavior, was developed in this study. The salient results are summarized below.

1) Tailoring the reaction conditions of the sol–gel process facilitated the formation of silica-coated copper microparticles with high potassium concentrations within the shell. Potassium hydroxide served as the catalyst and potassium source and prevented the formation of copper tetraamine complexes.
2) Selective metallization was performed on the Cu–PEEK composite surface using laser irradiation to generate conductive tracks in a single step. The electrical conductivity of the conductive tracks depended on the selected laser parameters, with the laser power and writing speed having the most significant influences. Increasing the laser power led to a decrease in the electrical resistance; in contrast, increasing the writing speed led to an increase in the electrical resistance.
3) The laser treatment enabled pyrolysis of the PEEK polymer and fusion of the copper particles into larger units. In addition, the laser parameters were selected to ensure that a metallized conductive track with a smooth surface was obtained.
4) The concentration and size of copper particles in the composite had a substantial impact on the thermal conductivity. The higher the copper concentration and smaller the particle size, the higher the thermal conductivity.
5) The Cu–PEEK composite was confirmed to be a suitable base material for generating conductive tracks via laser metallization.

Supporting Information

Supporting Information is available from the Wiley Online Library or from the author.

Acknowledgements

This study was funded by the Deutsche Forschungsgemeinde under Germany's Excellence Strategy program at the Cluster of Excellence PhoenixD (Leibniz Universität Hannover; EXC 2122, Project ID 390833453).

Open access funding enabled and organized by Projekt DEAL.

Conflict of Interest

The authors declare no conflict of interest.

Data Availability Statement

The data that support the findings of this study are available from the corresponding author upon reasonable request.

Keywords

copper, laser direct structuring, polyether ether ketone, sol–gel, thermal conductivity

Received: July 26, 2023
Revised: October 9, 2023
Published online: October 27, 2023

[1] J. Zhang, T. Zhou, L. Wen, A. Zhang, *ACS Appl. Mater. Interfaces* **2016**, *8*, 33999.
[2] a) Y. Li, Y. Wu, B. S. Ong, *J. Am. Chem. Soc.* **2005**, *127*, 3266; b) Y.-C. Liao, Z.-K. Kao, *ACS Appl. Mater. Interfaces* **2012**, *4*, 5109.

 © 2023 The Authors. Macromolecular Materials and Engineering published by Wiley-VCH GmbH

14392054, 2024, 2, Downloaded from https://onlinelibrary.wiley.com/doi/10.1002/mame.202300264 by Cochrane Germany, Wiley Online Library on [08/03/2024]. See the Terms and Conditions (https://onlinelibrary.wiley.com/terms-and-conditions) on Wiley Online Library for rules of use; OA articles are governed by the applicable Creative Commons License

Macromolecular Materials and Engineering
Open Access
www.mame-journal.de

[3] a) R. A. Ilyas, S. M. Sapuan, M. R. M. Asyraf, D. A. Z. N. Dayana, J. J. N. Amelia, M. S. A. Rani, M. N. F. Norrrahim, N. M. Nurazzi, H. A. Aisyah, S. Sharma, M. R. Ishak, M. Rafidah, M. R. Razman, *Polymers* **2021**, *13*, 1701; b) N. F. Zaaba, H. Ismail, A. M. Saeed, *Polym.-Plast. Technol. Mater.* **2021**, *60*, 1033; c) N. M. Sofian, M. Rusu, R. Neagu, E. Neagu, *J. Thermoplast. Compos. Mater.* **2001**, *14*, 20.
[4] a) S. Bhanushali, N. N. Jason, P. Ghosh, A. Ganesh, G. P. Simon, W. Cheng, *ACS Appl. Mater. Interfaces* **2017**, *9*, 18925; b) C. Liu, M. Chen, D. Zhou, D. Wu, W. Yu, *J. Nanomater.* **2017**, *12*, 6375135; c) X.-J. Wang, L.-Z. Zhang, L.-X. Pei, *J. Appl. Polym. Sci.* **2014**, *131*, 39550.
[5] E. Hahm, A. Jo, E. J. Kang, S. Bock, X.-H. Pham, H. Chang, B.-H. Jun, *Int. J. Mol. Sci.* **2021**, *22*, 11983.
[6] a) D. Vasudevan, R. R. Gaddam, A. Trinchi, I. Cole, *J. Alloys Compd.* **2015**, *636*, 395; b) A. Guerrero-Martínez, J. Pérez-Juste, L. M. Liz-Marzán, *Adv. Mater.* **2010**, *22*, 1182; c) L. P. Singh, S. K. Bhattacharyya, R. Kumar, G. Mishra, U. Sharma, G. Singh, S. Ahalawat, *Adv. Colloid Interface Sci.* **2014**, *214*, 17; d) Y. Kobayashi, M. Horie, M. Konno, B. Rodríguez-González, L. M. Liz-Marzán, *J. Phys. Chem. B* **2003**, *107*, 7420.
[7] Y. Kobayashi, H. Katakami, E. Mine, D. Nagao, M. Konno, L. M. Liz-Marzán, *J. Colloid Interface Sci.* **2005**, *283*, 392.
[8] S. Liu, Z. Zhang, M. Han, *Anal. Chem.* **2005**, *77*, 2595.
[9] a) S. Chen, M. Su, C. Zhang, M. Gao, B. Bao, Q. Yang, B. Su, Y. Song, *Adv. Mater.* **2015**, *27*, 3928; b) S. Magdassi, A. Bassa, Y. Vinetsky, A. Kamyshny, *Chem. Mater.* **2003**, *15*, 2208; c) P. Mei, T. N. Ng, R. A. Lujan, D. E. Schwartz, S. Kor, B. S. Krusor, J. Veres, *Appl. Phys. Lett.* **2014**, *105*, 123301.
[10] K.-T. Wang, W.-Y. Wang, T.-C. Wei, *ACS Omega* **2019**, *4*, 7706.
[11] a) M. Berggren, D. Nilsson, N. D. Robinson, *Nat. Mater.* **2007**, *6*, 3; b) S. Chung, M. A. Ul Karim, H.-J. Kwon, V. Subramanian, *Nano Lett.* **2015**, *15*, 3261; c) R. P. Gandhiraman, V. Jayan, J.-W. Han, B. Chen, J. E. Koehne, M. Meyyappan, *ACS Appl. Mater. Interfaces* **2014**, *6*, 20860.
[12] a) A. Garcia, J. Polesel-Maris, P. Viel, S. Palacin, T. Berthelot, *Adv. Funct. Mater.* **2011**, *21*, 2096; b) A. Garcia, T. Berthelot, P. Viel, A. Mesnage, P. Jégou, F. Nekelson, S. Roussel, S. Palacin, *ACS Appl. Mater. Interfaces* **2010**, *2*, 1177; c) A. Garcia, T. Berthelot, P. Viel, J. Polesel-Maris, S. Palacin, *ACS Appl. Mater. Interfaces* **2010**, *2*, 3043.
[13] H. Xu, J. Zhang, J. Feng, T. Zhou, *Ind. Eng. Chem. Res.* **2021**, *60*, 8821.
[14] J.-U. Yang, J. H. Cho, M. J. Yoo, *Composites, Part B* **2017**, *110*, 361.
[15] S. Najeeb, M. S. Zafar, Z. Khurshid, F. Siddiqui, *J. Prosthodont. Res.* **2016**, *60*, 12.
[16] a) S. Tencé-Girault, J. Quibel, A. Cherri, S. Roland, B. Fayolle, S. Bizet, I. Iliopoulos, *ACS Appl. Polym. Mater.* **2021**, *3*, 1795; b) A. Ben-Haida, H. M. Colquhoun, P. Hodge, D. J. Williams, *Macromolecules* **2006**, *39*, 6467; c) A. Cherri, I. Iliopoulos, G. Régnier, B. Brulé, G. Lé, S. Tencé-Girault, *ACS Appl. Polym. Mater.* **2022**, *4*, 2806.
[17] a) X. Han, D. Yang, C. Yang, S. Spintzyk, L. Scheideler, P. Li, D. Li, J. Geis-Gerstorfer, F. Rupp, *J. Clin. Med.* **2019**, *8*, 240; b) D. Veazey, T. Hsu, E. D. Gomez, *J. Appl. Polym. Sci.* **2017**, *134*, 44441; c) L. Miller, M. Juza, *J. Chromatogr. A* **2005**, *1094*, 165.
[18] L. Qin, S. Yao, J. Zhao, C. Zhou, T. W. Oates, M. D. Weir, J. Wu, H. H. K. Xu, *Materials* **2021**, *14*, 408.
[19] a) G. Colucci, C. Beltrame, M. Giorcelli, A. Veca, C. Badini, *RSC Adv.* **2016**, *6*, 28522; b) N. Bityurin, B. S. Luk'yanchuk, M. H. Hong, T. C. Chong, *Chem. Rev.* **2003**, *103*, 519; c) I.-B. Sohn, Y.-C. Noh, S.-C. Choi, D.-K. Ko, J. Lee, Y.-J. Choi, *Appl. Surf. Sci.* **2008**, *254*, 4919.
[20] L. Pan, U. Yapici, *Adv. Compos. Mater.* **2016**, *25*, 359.
[21] S. I. Shornikov, *Exp. Geosci.* **2013**, *19*, 108.
[22] T. Ung, L. M. Liz-Martin, P. Mulvaney, *Langmuir* **1998**, *14*, 3740.
[23] A. E. Danks, S. R. Hall, Z. Schnepp, *Mater. Horiz.* **2016**, *3*, 91.
[24] L. M. Liz-Marzán, M. Giersig, P. Mulvaney, *Langmuir* **1996**, *12*, 4329.
[25] a) E. Mine, A. Yamada, Y. Kobayashi, M. Konno, L. M. Liz-Marzán, *J. Colloid Interface Sci.* **2003**, *264*, 385; b) G. H. Bogush, M. A. Tracy, C. F. Zukoski IV, *J. Non-Cryst. Solids* **1988**, *104*, 95.
[26] O. Malay, I. Yilgor, Y. Z. Menceloglu, *J. Sol-Gel Sci. Technol.* **2013**, *67*, 351.
[27] Z. Lu, T. Zhang, Z. Liu, X. Kong, Z. Sun, *J. Appl. Polym. Sci.* **2023**, *140*, e53310.
[28] K. Sinkó, *Materials* **2010**, *3*, 704.
[29] A. V. Dolmatov, S. S. Maklakov, P. A. Zezyulina, A. V. Osipov, D. A. Petrov, A. S. Naboko, V. I. Polozov, S. A. Maklakov, S. N. Starostenko, A. N. Lagarkov, *Sensors* **2021**, *21*, 4624.
[30] G. D.a C. Vasconcelos, R. L. Mazur, B. Ribeiro, E. C. Botelho, M. L. Costa, *Mater. Rep. (Aust., Aeronaut. Res. Lab.)* **2014**, *17*, 227.
[31] P. Patel, T. R. Hull, R. W. McCabe, D. Flath, J. Grasmeder, M. Percy, *Polym. Degrad. Stab.* **2010**, *95*, 709.
[32] A. M. Salaberria, J. Labidi, S. C. M. Fernandes, *Chem. Eng. J.* **2014**, *256*, 356.
[33] D. H. Droste, A. T. Dibenedetto, *J. Appl. Polym. Sci.* **1969**, *13*, 2149.
[34] J. Atkinson, *Polymer* **2002**, *43*, 731.
[35] A. Z. Al-Khazaal, N. Ahmad, *Eng. Technol. Appl. Sci. Res.* **2022**, *12*, 8555.
[36] a) L. Simonin, H. Liao, *Macromol. Mater. Eng.* **2000**, *283*, 153; b) V. S. Rangasamy, S. Thayumanasundaram, N. de Greef, J. W. Seo, J.-P. Locquet, *Solid State Ionics* **2012**, *216*, 83.
[37] A. Caradonna, C. Badini, E. Padovano, A. Veca, E. de Meo, M. Pietroluongo, *Micromachines* **2019**, *10*, 63.
[38] J. Liu, P. Wen, *Mater. Des.* **2022**, *215*, 110505.
[39] S. Hou, S. Qi, D. A. Hutt, J. R. Tyrer, M. Mu, Z. Zhou, *J. Mater. Process. Technol.* **2018**, *254*, 310.
[40] a) F. Lupone, E. Padovano, A. Veca, L. Franceschetti, C. Badini, *Mater. Des.* **2020**, *193*, 108869; b) E. Padovano, M. E. Bonelli, A. Veca, E. de Meo, C. Badini, *React. Funct. Polym.* **2020**, *152*, 104601.
[41] W. Yuan, H. Chen, T. Cheng, Q. Wei, *Mater. Des.* **2020**, *189*, 108542.
[42] A. Caradonna, F. Tagliafierro, A. Veca, C. Badini, *Polym. Eng. Sci.* **2018**, *58*, 1485.
[43] L. Rivière, A. Lonjon, E. Dantras, C. Lacabanne, P. Olivier, N. R. Gleizes, *Eur. Polym. J.* **2016**, *85*, 115.
[44] B. Ghosh, F. Xu, X. Hou, *J. Mater. Sci.* **2021**, *56*, 10326.
[45] S. Zhang, X. Y. Cao, Y. M. Ma, Y. C. Ke, J. K. Zhang, F. S. Wang, *eX-PRESS Polym. Lett.* **2011**, *5*, 581.

 © 2023 The Authors. Macromolecular Materials and Engineering published by Wiley-VCH GmbH

14392054, 2024, 2, Downloaded from https://onlinelibrary.wiley.com/doi/10.1002/mame.202300264 by Cochrane Germany, Wiley Online Library on [08/03/2024]. See the Terms and Conditions (https://onlinelibrary.wiley.com/terms-and-conditions) on Wiley Online Library for rules of use; OA articles are governed by the applicable Creative Commons License